How thermal stability of ionic liquids leads to more efficient TiO$_2$-based nanophotocatalysts: Theoretical and experimental studies

Anna Rybińska-Fryca[a,#], Alicja Mikolajczyk[a,#,*], Justyna Łuczak[b,*], Marta Paszkiewicz-Gawron[c], Monika Paszkiewicz[d], Adriana Zaleska-Medynska[c], Tomasz Puzyn[a]

a)   Laboratory of Environmental Chemometrics, Faculty of Chemistry, University of Gdan´sk, Wita Stwosza 63, 80-308 Gdańsk, Poland

b)   Department of Process Engineering and Chemical Technology, Chemical Faculty, Gdańsk University of Technology, Narutowicza 11/12, 80-233 Gdańsk, Poland

c)   Department of Environmental Technology, Faculty of Chemistry, University of Gdańsk, Wita Stwosza 63, 80-308 Gdańsk, Poland

d)   Department of Environmental Analysis, Faculty of Chemistry, University of Gdańsk, Wita Stwosza 63, 80-308 Gdańsk, Poland

*Corresponding authors:

E-mail addresses: alicja.mikolajczyk@ug.edu.pl (A. Mikolajczyk), justyna.luczak@pg.gda.pl (J. Łuczak).

#These authors contributed equally.

Abstract

Ionic liquids (ILs) containing distinct nitrogen-bearing organic cations (pyridinium, pyrrolidinium, imidazolium, ammonium, morpholinium) were first used for the preparation of 23 IL-TiO$_2$ types of composites by ionic liquid assisted solvothermal synthesis. These 23 optimal ILs structures (i.e. compounds exhibiting an optimal combination of specific properties, functionality, and safety) for synthesis and experimental validation were selected by computational high-throughput screening from a combinatorically created library containing 836 ILs theoretically designed and characterized candidates. Then, selected IL-TiO$_2$ structures with potential photocatalytic activity were synthesized with the use of solvothermal reaction. Then, the decomposition level, the role of the individual IL cation structure on the morphology, thermal stability, surface and photocatalytic properties of the IL-TiO$_2$ microparticles were determined experimentally. The chemoinformatic analysis of the relationship between the structure of the ionic liquid, its thermal stability under the conditions of synthesis and photocatalytic activity was applied for the first time. The results presented here are the first step in the development of methodology (combined experimental and theoretical) that may simplify the procedure of designing safer and more efficient TiO$_2$-based photocatalyst. The developed computational methodology makes it possible to predict properties of newly synthesized IL-TiO$_2$ materials before synthesis and identifies structural features of ILs that influence the efficiency of IL-TiO$_2$ system. The presented approach reduces the number and cost of necessary experiments, as well as increases the success ratio of efficient TiO$_2$-based photocatalyst design by a selection of optimal IL structures (i.e. ionic liquid characterized by a combination of most promising physicochemical features).

1. Introduction

The importance of semiconductor photocatalysis in fundamental and applied research is well known and reported in numerous studies and reviews concerning various types of materials [1–10]. For practical applications of this process, usage of solar irradiation as an energy source is crucial, therefore, many studies were devoted to extending the absorption range to the visible (Vis) and near infra-red regions, and to limit at the recombination of photogenerated charge carriers [11−13]. However, Vis light driven photocatalytic reactions are dictated by the thermodynamic and kinetic requirements, smaller energy of irradiation with longer wavelength results in decreased in the potential for redox reactions. Strategies usually use in research on titanium dioxide (a representative photocatalyst used in this research) to achieve wavelength extension employ: (i) surface modification of the semiconductor by organic compounds (sensitizers or surface complexes forming substances) or metal nanoparticles, (ii) combining with narrow band gap semiconductor, or (iii) structure alteration by doping [14−16]. However, recent publications suggest using ionic liquids (ILs), as solvents/functional compounds, for preparation of titania, since ILs are able to both determine the morphology and enhance photoactivity of the semiconductor under Vis irradiation [17−21]. Ionic liquids, being salts liquid below 100°C composed of large organic cation and inorganic/organic anion (some examples are shown in Fig. 1), participate in numerous attractive interactions (Coulombic forces, van der Waals, dispersive, solvophobic, p-p interactions, hydrogen, halogen bonding) [17,18].
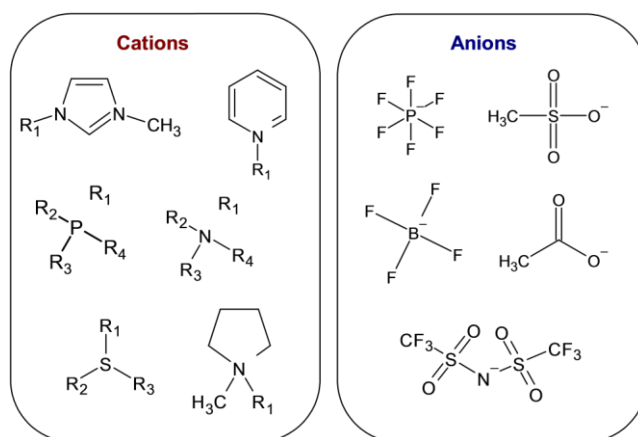

Fig. 1. Examples of ions that could build ionic liquid (cations from left: imidazolium, pyridinium, phosphonium, ammonium, sulphonium, pyrrolidinium; Anions from left: hexafluoro-phosphate, methanesulfonate, tetrafluoroborate, acetate, bis (trifluoromethylsulfonyl).

The interplay of the interactions makes ILs an important key tool in the preparation of nano- and microstructures with different morphologies [21,22]. It is widely believed that the real strength of ILs is related to the possibility to modify the cation and anion structure (ILs are frequently termed "designer solvents"), and as a consequence to alter their physicochemical properties as well as possible interactions between IL and solute [23,24]. In this regard, ILs with specific, chosen properties can be used to synthesize new materials (e.g. titania) with expected morphologies and functions [25].

Preliminary results revealed that IL-TiO$_2$ photocatalytic activity depends on the IL structure and its stability [26]. The ionic liquids could lead to visible light absorption and Vis-driven activity of TiO$_2$ due to one of the following mechanisms: (i) by creating a surface complex between IL and TiO$_2$, or (ii) by creating of mid-bandgap level in TiO$_2$ induced by nonmetal atoms doping, originated from the ionic liquid (Fig. 2). The effect of ionic liquids on morphology and photoactivity of TiO$_2$ was proved and

described in detail in previous studies by Paszkiewicz et al. [27], Luczak et al. [25], Paszkiewicz-Gawron et al. [26,28], Gołąbiewska et al. [29,30].

The way in which the ionic liquid interacts with TiO$_2$ depends on its durability (decomposition level) under the conditions of TiO$_2$ synthesis. Thus, stable ionic liquids (not decomposed during solvothermal synthesis) could be involved in the formation of a charge-transfer (CT) complex between TiO$_2$ and IL (surface adsorbate). According to this mechanism (referred to the Creutz–Brunch wig–Sutin model), the photoexcited electron may be transferred from IL in the ground state (the excited state of the adsorbate is not involved) to the conduction band of TiO$_2$ [31–33]. In this regard, new energy levels may be formed between TiO$_2$ and the anion of IL (where HOMO orbital is usually located) [26]. Moreover, one electron from the free electron pair on the halide anion (derived from IL) migrates into the ρ* of molecular oxygen orbital, thus forming the superoxide anion radicals O2$^-$ which can reduce the impurities present on the surface of the TiO$_2$ particles [25]. Contrarily, ionic liquids that are completely or partially decomposed could serve as a source of non-metallic species incorporated (doped) into TiO$_2$ structure. Thus, decomposition of N-containing IL resulting in the formation of Ti–Nx species (interaction of N atoms with deeper sites of TiO$_2$). As a consequence, the additional energy states are created (N2p) above O2p valence band, from which electrons can be transferred to the conduction band resulting in an increase of the absorption properties under visible irradiation [26].
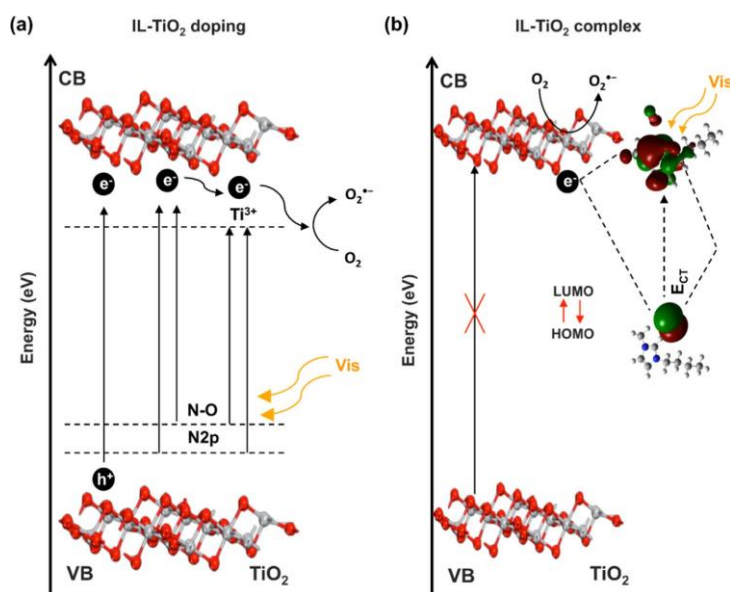

Fig. 2. The two possible mechanisms of photoexcitation under visible irradiation (k > 420 nm) for TiO$_2$ samples modified with ionic liquids.

Summing up, there is a possible linkage between mechanism of photoexcitation under Vis and the chemical structure and degree of ILs decomposition. However, the number of potential ILs is enormous and was estimated to be as high as 10^{18} salts (not including IL mixtures). It is simply not realistic and unreasonable to take into account all of them or easily choose one and expect an improved outcome. Random selection will not necessarily provide the desired effect. Therefore, results and knowledge from our previous studies was used on TiO$_2$-IL systems and extend by adding theoretical studies to improve the procedure of designing a more efficient TiO$_2$-based photocatalyst. For this reason, our research focus on three areas (Fig. 3). Firstly, creating a virtual library of 836 combinatorically created and theoretically characterized ILs structures (candidates). Secondly, the selection of most promising ILs structures for efficient TiO$_2$-based photocatalyst synthesis (i.e. compounds exhibiting an optimal combination of

specific properties, functionality and safety). Thirdly, chemoinformatic analysis of the relationship between the structure of the ionic liquid and its thermal stability under the conditions of synthesis.
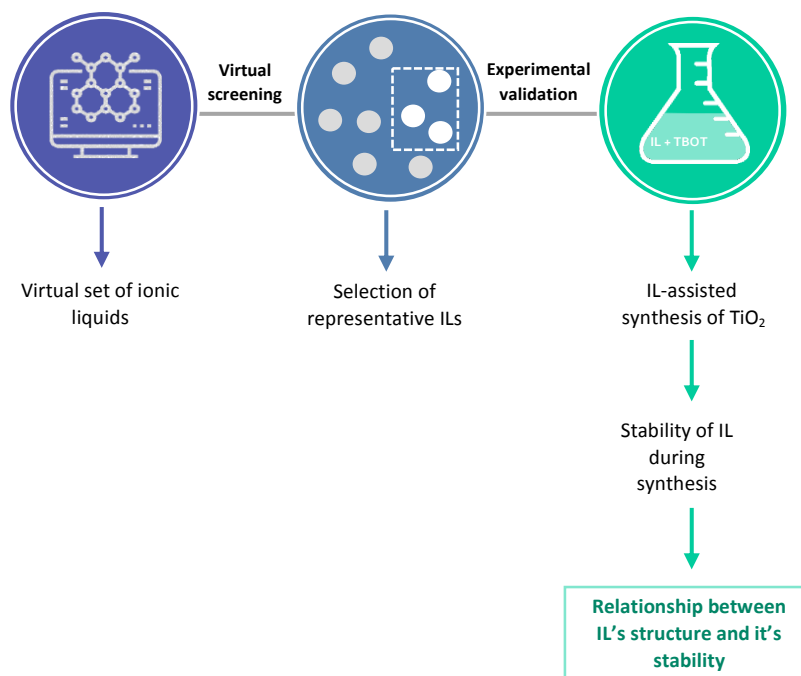

Fig. 3. Schematic representation of the performed study.

2. Experimental section

Solvothermal synthesis

The IL-assisted samples were synthesized as follows: titanium (IV) n-butoxide (TBOT, Sigma Aldrich) was dissolved in absolute ethanol (Sigma Aldrich), and then HCl (Sigma Aldrich), distilled water and different types of IL were added. Ionic liquids were provided by Sigma Aldrich or Iolitec. Next, the mixture was transferred to a 200 mL Teflon-lined stainless-steel autoclave and kept at 180°C for 24 h. Upon the completion of the reaction, the autoclave was cooled to room temperature, and the product washed with ethanol and deionized water and dried at 50°C for 6 h. Thereafter, the samples were calcined for 2 h at 200°C. Pristine TiO_2 was prepared, as the reference system, using the same method but without IL addition.

Structure, morphology and absorption properties of IL-TiO_2 samples

The IL-assisted TiO_2 samples morphology, size and properties (e.g. crystal structure, average crystallite size, specific surface area, surface composition, optical properties and stability in photocatalytic reaction) were investigated and discussed in previous experimental papers [25–30]. All the information was gathered and can be found in Supplementary Information (Table S1).

Decomposition of ionic liquid

The decomposition level of cations was analyzed using HPLC or LC-MS (depending on the ionic liquid cation structure – supplementary data). HPLC (Shimadzu) was used system equipped with a diode array detector SPD-M20A, pump LC-20AD, autosampler SIL 20AHT, column oven CTO-10ASvp and degasser DGU-20A5R. HPLC-grade acetonitrile with addition of 0.025% trifluoroacetic acid (v/v) and deionized water containing 0.025% TFA (v/v) were used as a mobile phase A and B, respectively. The separation was carried out with Hypersil Gold aQ column 150 x 4.6; 5 μm (Thermo Scientific, Waltham) and an isocratic (5 % of mobile phase A and 95% of phase B) or gradient elution mode (from 30% to 90% ofmobile phase A) was used depending on the structure of ILs.. The flow rate was 1 mL min^{-1}, and the elution profiles were monitored at 205 nm or 258 nm. Each sample (before and after solvothermal reaction) was measured in triplicate. Agilent 1200 Series LC system (Agilent Technologies, Inc., Santa Clara, USA) was coupled to HCT ultra ion trap mass spectrometer (Bruker Daltonics, Bremen, Germany) with an electrospray ionization (ESI) source. The mass spectrometer was operated in the positive ion mode using a capillary voltage of 4.0 kV. Ions with m/z 50–400 were monitored in a full scan mode. Nitrogen was employed as the nebulizer gas (30 psi) and the dry gas (10 L min^{-1}). Analyses were performed using a Thermo Hypersil Gold aQ 150 x 4.6; 5 μm column (150 mm x 4.6 mm, 5 μm). The mixture of acetonitrile (10 %, v/v) with 5 mM ammonium acetate buffer in deionized water was used as mobile phase. The flow rate of mobile phase was 0.4 mL min^{-1}. Each sample (before and after solvothermal reaction) was measured in triplicate. The decomposition level of cations was calculated as:

$$\eta IL(\%) = 100 \times C_0 - \left(\frac{C}{C_0}\right)$$

where: C_0 is the initial concentrations of cations of ILs; C is the concentrations of cations of ILs after the solvothermal reaction.

Photocatalytic activity determination

The photocatalytic activity of the IL-TiO$_2$ semiconductors was determined in a model reaction of the phenol decomposition in an aqueous solution under visible irradiation. The experiment was performed in a cylindrical reactor with a quartz window where 0.125 g of the photocatalysts in 25 mL of phenol solution (0.21 mmol) was suspended. The aeration (5 dm^3/h) and stirring of the dispersion were kept prior to and during the photocatalytic process. The photoirradiation was provided by a 1000 W Xenon lamp (6271H, Oriel), capable of emitting both, the UV and Vis light. To perform the experiments under visible irradiation, an optical filter (k > 420 nm) was used. Before the illumination as well as during the degradation process 1 cm^3 aliquot of the aqueous suspension were sampled. Before analysis, the fine particles of the photocatalyst were removed by filtering through a 0.2 mm syringe filter. To determine the phenol concentration, the colorimetric method was used (spectrophotometer Spectro UV–VIS Double Beam Spectrometer UVD-3500 Labmed, Inc.). The efficiency of phenol photolysis, as well as, the amount of analyte adsorbed on the photocatalyst surface in the dark condition was investigated in our previous study by the blind test (phenol degradation experiments in the absence of illumination or photocatalyst) that proceeded main degradation runs. Phenol degradation was not observed in both conditions [28].

3. Modeling of thermal stability of ionic liquids

Selection of the representative ionic liquids for synthesis

The presented procedure for the built-by-design of TiO_2 particles with the expected properties consists of several steps. At first, a database of possible derivatives of a variety of cations was generated (ammonium, imidazolium, phosphonium, sulfonium, pyridinium, piperidinium, pyrrolidinium, thiazolium). Following this, the molecular descriptors (numerical representation of molecular structures) were calculated for each generated ion in the Dragon and Padel software [34,35]. However, only selected descriptors were used in further analysis, namely: nN (number of nitrogen atoms), nP (number of phosphorous atoms), nS (number of sulfur atoms), nHDon (number of donor atoms for H-bonds (N and O)), nHAcc (number of acceptor atoms for H-bonds (N,O,F), Sv (sum of atomic van der Waals volumes (scaled on Carbon atom)), Wap (all-path Wiener index), nClC (number of rings (cyclomatic number)), nAtomLAC (number of atoms in the longest aliphatic chain). Additionally, the nature of the cation (protic or aprotic) was considered.

Subsequently, the hierarchical clustering algorithm (HCA) was used to divide the cationic structures into several groups. Hierarchical clustering is an iterative method of grouping objects (cations) into a tiered, ordered structure that can be used to explore the data and visualize their underlying structure. All clustering methods are built on the concept of similarity: the greater the distance between objects, the lesser their similarity [36]. In the case of the presented study, the distance between objects was defined by the Euclidean metric. The proximity between two clusters, or an object and an already formed cluster was measured in accordance with the Ward linkage (minimum variance method in which the proximity of clusters is calculated as the Euclidean distance between their centroids multiplied by a correction factor) [37,38]. Then, the representative cationic structures from every group were selected. Finally, the potential ionic liquids were formed by combining selected cations with several anions like chloride, bromide, iodide, and hexafluorophosphate.

Database of molecular descriptors

To obtain numerical variables that characterize chemical structures, the molecular models of all selected cations and anions from the studied dataset were created by using the ChemSketch software [39]. Then, each ion was described by the set of descriptors called molecular fingerprints (FPs). They encode the structural information within a molecule as a bit vector (also known as bit string or Boolean array). It is a sequence of bits, where a bit equal 0 indicates the absence of a structural feature corresponding to the bit at a given position. Bit equals 1 and expresses the presence of a particular molecular feature (Fig. 4). Such representation of the molecular structure allows for efficient comparison of chemical compounds. Therefore, we can perform virtual screening of large datasets. Moreover, we can easily identify compounds ("neighbors") that could have a similar level of biological activity or physicochemical properties [40,41].There are several available FPs, differing in the set of keys (predefined substructures) used for their generation, e.g., MACCS FP, Klekota– Roth FP (KR), Substructure FP (SUB), or CACTVS FP (or PubChem FP) [42]. In this study, the Klekota–Roth and substructure fingerprints were used. It should be noted, that the preprocessing step was carried out. All variables with constant values were excluded.
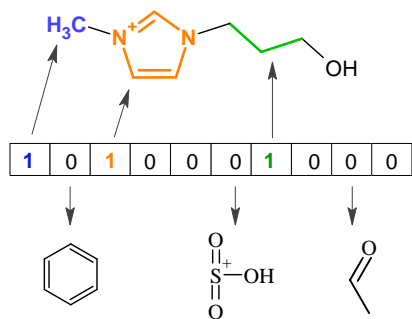
Fig. 4. Schematic representation of a molecular fingerprint.

Chemometric analysis

The Principal Coordinates Analysis (PCoA) was employed to visualize the studied dataset and investigate possible patterns and similarities of the ionic liquids. PCoA is one of the methods that have commonly been used for mapping high dimensional datasets in the low-dimensional representations [43]. The input to PCoA is a dissimilarity matrix D which element contain dissimilarity indices calculated using one of the distance metrics (e.g. Euclidean, Chebyshev, Rogers and Tanimoto, etc.). In this study, the Jaccard distance also known as the similarity ratio was used. Once the dissimilarity matrix is calculated, the following steps are executed: [44,45].

1. Transformation of D matrix into A accordingly to the equation:

$$A = \left(-\frac{1}{2}\right) \times D^2$$

$$a_{ij} = \left(-\frac{1}{2}\right) \times d_{ij}^2$$

2. Calculation of a column and row centered H matrix:

$$h_{ij} = a_{ij} - a_i - a_j + a$$

where a_i and a_j represent the row and column means for sample i and variable j of matrix A and the overall mean.

3. Performing the Principal Component Analysis:

$$H = TP + E$$

where TP can be reformulated as TP = P`Λ1/2 where Λ is a matrix whose diagonals contain the square root of the eigenvalues of the PCs.

The Principal Coordinates Analysis was performed in the space of molecular fingerprints that characterize studied ILs. It was carried out by employing the ''stats'' package available in R programming language (R version 3.5.0) [46].

The decision tree classification algorithm was applied to predict the decomposition level of ionic liquids based on their structural features. The chosen method is one of the supervised learning techniques that can be used for classification as well as regression. The goal is to create a model that predicts the value of a target variable by learning simple decision rules [47]. Building the ''tree'' involves finding the feature that will partition the data into subsets that contains objects with similar values (structural properties). Objects are divided into separate branches when information gain has the highest value (entropy after splitting is equal to zero). The main advantages of decision trees are simplicity and easy interpretation. Moreover, it can be used for both numerical and categorical data [47,48]. In this study, the whole dataset (a matrix that contains information about decomposition level and molecular fingerprint for each ionic liquid) was randomly split into training and validation sets. The training set contained 20 data points (85% of all data points) and was used for model calibration. The validation set contains 3 data points and was used for assessing the predictive ability of the model (Table S2 in Supplementary Information). Then, the classification tree was grown with the R program using the rpart library with the following parameters: complexity parameter (cp) = 0.0301, the minimum number of observations that must exist in a node for a split to be attempted (minsplit) = 2. It should be highlighted that model development was based only on the 20 ILs from the training set.

Moreover, the developed model should fulfill quality criteria established by the Organization for Economic Co-operation and Development (OECD) [49]. In the case of classification techniques, several metrics should be calculated to establish model credibility [47]. First, the confusion matrix (contingency table) has to be prepared. It gives insight into the performance of a classification algorithm (Fig. 5). Secondly, the number of True Positives (TP), True Negatives (TN), False Positives (FP), and False Negatives (FN) samples should be established.

		Predicted value	
		High level	Low level
Observed value	High level	True positive (TP)	False positive (FP)
	Low level	False negative (FN)	True negative (TN)

Fig. 5. Confusion matrix describing the performance of a classification model on a set of data for which the true values are known.

Based on the confusion matrix the several metrics can be calculated. The most basic one is the overall percentage correctly classified (%CC). A high value indicates that the majority of samples were assigned to the correct group. Moreover, the sensitivity, specificity, accuracy, precision, and F-measure of a method can be evaluated:

$$sensitivity = \frac{TP}{(TP + FN)}$$

$$specificity = \frac{TN}{(FP + TN)}$$

$$accuracy = \frac{TP + TN}{(TP + FP + TN + FN)}$$

$$precision = \frac{TP}{(TP + FP)}$$

$$F_{measure} = \frac{2(sensitivity)(precision)}{(sensitivity + precision)}$$

All metrics were calculated for the training set. Additionally, the separate set, called validation set, was used to assess the predictive ability of the model. The developed model was used to predict the decomposition level of the three ILs from the validation set. Finally, the actual decomposition level was compared with predicted values, and all the mentioned quality metrics were calculated.

4. Results and discussion

To reduce the number of cationic structures for further selection of representative ionic liquids the hierarchical clustering algorithm (HCA) was performed. As a result, cations were grouped into nine clusters schematically described in Fig. 6. Each group differs from each other in terms of the structural properties of cations belonging to a given group. Next, the potential ionic liquids were formed by combining selected cations with several anions i.e. chloride, bromide, iodide, nitrate, and octyl sulfate, respectively. Then, selection of most promising ILs structures for efficient TiO$_2$-based photocatalyst synthesis was performed. Finally, chosen compounds were used for the preparation of IL-TiO$_2$ composites by ionic liquid assisted solvothermal synthesis.
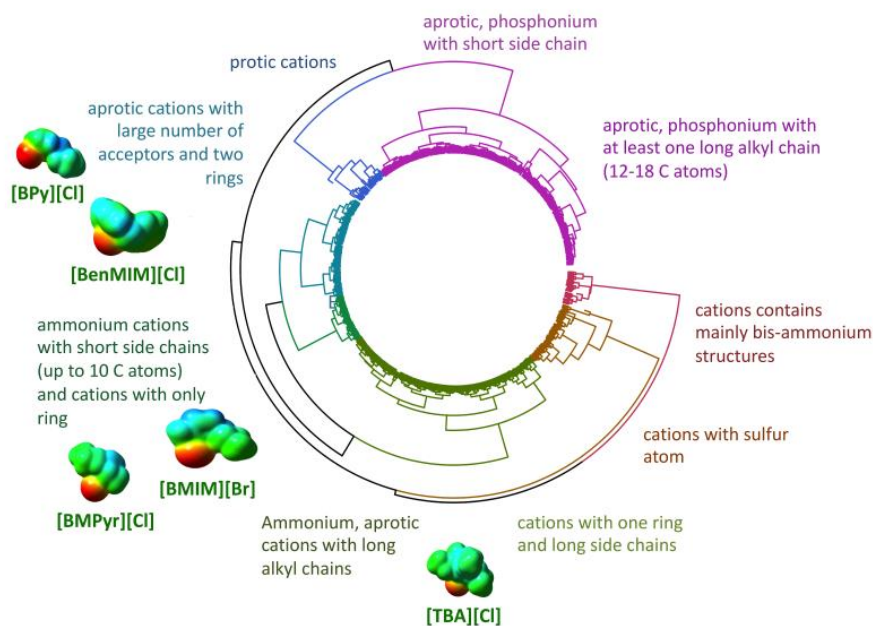

Fig. 1. The schematically represented Hierarchical Cluster Analysis (HCA) for selection of representative cations (optimal structures) for synthesis and preliminary experimental testing of ionic liquids

The experimental data including sample labels, effectiveness of IL decomposition during the IL-assisted solvothermal preparation route (η) as well as photoactivity (Δ) of the product are presented in Table 1. The photocatalysts with the highest

activity toward phenol degradation in each series (series comprises of a set of samples prepared for various IL:TBOT molar ratios) was taken into account. In this regard sample label included IL's abbreviation and IL:TBOT molar ratio presented in parenthesis. From the all studied ionic liquids, seven had decomposition level higher than 60%, the remaining ones were more persistent. The highest value of decomposition level (100%) during the solvothermal reaction conditions had 2,3,5-triphenyltetrazolium chloride (TPTZ). The IL-TiO$_2$ sample with the highest photoactivity was obtained when the IL:TBOT molar ratio equal to 1:10 was applied TiO2_TPTZ (1:10). The lowest values of decomposition level (0%) had four ionic liquids used in synthesis, namely 3-methyl-1tetradecylimidazolium chloride (TDMIM), 1-methyl-3octadecylimidazolium chloride (ODMIM), 1-butyl-1methylpyrrolidinium chloride (BMPyr), and tetrabutylammonium chloride (TBA). The decomposition levels for all studied samples can be found in Table 1 (Detailed information about samples can be found in Supplementary Information Table 1S).

Table 1 Photocatalytic activity of IL-TiO$_2$ samples

ID	Sample label	Ionic liquid	η [%]	Δ [%]
1	TiO$_2$_S222(1:1)	triethylsulfonium iodide	75	39[f]
2	TiO$_2$_BenMIM(1:2)	1-benzyl-3-methylimidazolium chloride	25	44[a]
3	TiO$_2$_BMIM(1:2)	1-butyl-3-methylimidazolium chloride	2	25[b]
4	TiO$_2$_DMIM(1:2)	1-decyl-3-methylimidazolium chloride	7	32[b]
5	TiO$_2$_TDMIM(1:3)	3-methyl-1-tetradecylimidazolium chloride	0	61[c]
6	TiO$_2$_DDMIM(1:10)	1,3-didecyl-2-methylimidazolium chloride	5	25[f]
7	TiO$_2$_ODMIM(1:3)	1-methyl-3-octadecylimidazolium chloride	0	59[c]
8	TiO$_2$_BPy(1:3)	1-butylpyridinium chloride	50	58[a]
9	TiO$_2$_BMPyr(1:5)	1-butyl-1-methylpyrrolidinium chloride	0	49[a]
10	TiO$_2$_TBA(1:2)	tetrabutylammonium chloride	0	46[a]
11	TiO$_2$_MIM(1:1)	1-methylimidazolium chloride	80	53[f]
12	TiO$_2$_EANCl(1:1)	ethylammonium chloride	29	43[f]
13	TiO$_2$_NH(1:8)	hexylammonium iodide	20	42[f]
14	TiO$_2$_EAN(1:1)	ethylammonium nitrate	97	88[d]
15	TiO$_2$_BMIMBr(1:2)	1-butyl-3-methylimidazolium bromide	12	40[e]
16	TiO$_2$_BMIMOct(1:2)	1-butyl-3-methylimidazolium octylsulfate	4	21[e]
17	TiO$_2$_TPTZ(1:10)	2,3,5-triphenyltetrazolium chloride	100	74[f]
18	TiO$_2$_BMMTDA(1:3)	benzyldimethyltetradecylammonium chloride	95	17[f]
19	TiO$_2$_HDPyrCl	hexadecylpyridinium chloride	12	91[f]
20	TiO$_2$_TBMA(1:2)	tributylmethylammium chloride	93	79[f]
21	TiO$_2$_HOEtMIM(1:1)	1-(2-hydroxyethyl)-3-methylimidazolium chloride	14	53[f]
22	TiO$_2$_Chol(1:1)	(2-Hydroxyethyl)trimethylammonium chloride	49	54[f]
23	TiO$_2$_BMMor(1:2)	N-butyl-N-methylmorpholinium chloride	95	34[f]
24	Unmodified TiO$_2$		-	13[a]

η – decomposition; Δ - photodegradation

a) Paszkiewicz-Gawron M et al., ACS Sustainable Chemistry & Engineering, 6 (2018) 3927-3937;

b) Paszkiewicz M., et al, Applied Catalysis B: Environmental, 184 (2016) 223-237;

c) Gołąbiewska A., et al., Beilstein Journal of Nanotechnology, 9 (2018) 580-590;

d) Gołąbiewska A., et al., Catalysts 8 (2018) 279;

e) Łuczak J., et al.,ChemCatChem, 9 (2017) 4377-4388

f) this work

As mentioned, each ionic liquid was described by a set of molecular fingerprints that encode the structural information about cationic and anionic moieties (separately). In consequence, the twenty-three chemicals were characterized by a set of 13 substructural and set of 45 Klekota–Roth fingerprints. Detailed information about the dataset can be found in Supplementary Information Table 2S. The application of PCoA analysis performed for the compounds in the space of those two sets of descriptors allows visualizing the structural similarity between ionic liquids. In the case of substructural fingerprints, four groups were observed, each one with different levels of ionic liquids decomposition (Fig. 7). For example, ethylammonium chloride (EANCl) (depicted in Fig. 7 as 12) decomposed only in 29%, thus decomposition level is low. In contrast, the decomposition level of ethylammonium nitrate (EAN) (14) was very high (97%). Based on these results, we assumed that substructure fingerprints are not sufficient for further analysis. In the case of the Klekota–Roth fingerprints, ionic liquids formed nine groups. However, not all of them were heterogenic (Fig. 8). There are two homogenous groups that contain ionic liquids only with low level of decomposition: 1-butyl3-methylimidazolium chloride (BMIM) (3), 1-decyl-3- methylimidazolium chloride (DMIM) (4), 3-methyl-1-tetradecylimidazolium chloride (5), 1,3-didecyl-2-methylimidazolium chloride (DDMIM) (6), 1-methyl-3-octadecylimidazolium chloride (7), 1-butylpyridinium chloride (BPy) (8), 1-butyl-3methylimidazolium bromide (BMIMBr) (15), 1-butyl-3-methylimidazolium octylsulfate (BMIMOct) (16), hexa-decylpyridinium chloride (HDPyr) (19). We concluded that the Klekota–Roth fingerprints encode structural fragments that influence the decomposition level. Thus, they were more suitable for model development than substructure fingerprints. Nevertheless, to verify whether the application of both sets will improve the mapping, we ionic liquids was visualize in space of both sets of descriptors simultaneously. As shown in Fig. 9, the number of homogenous groups has not changed. However, two ionic liquids with different decomposition levels (1 and 21) were separated in a better way. Based on the results presented in Figs. 7 and 9, both sets were used in the process of the classification model development.
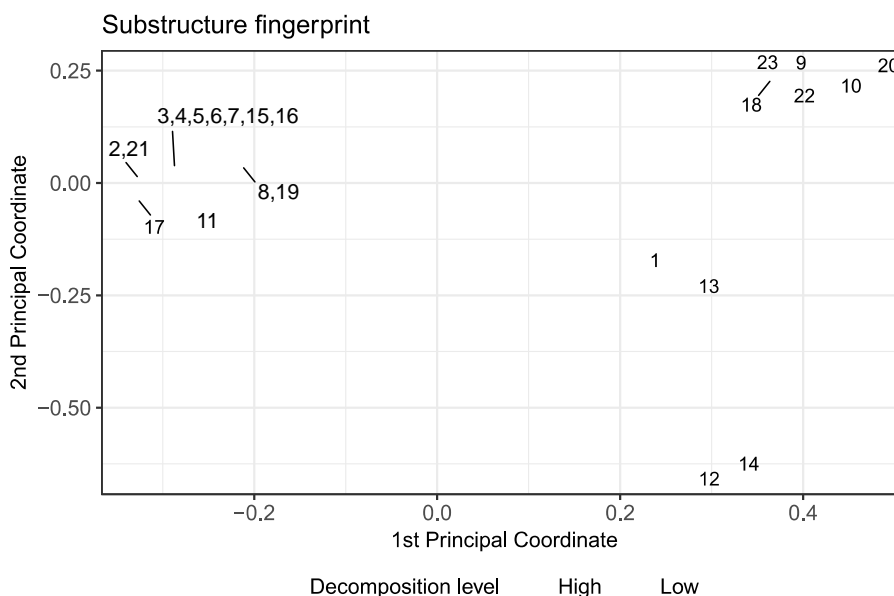

Fig. 2. Score plot illustrating location of the compounds in the space of the Substructure fingerprint
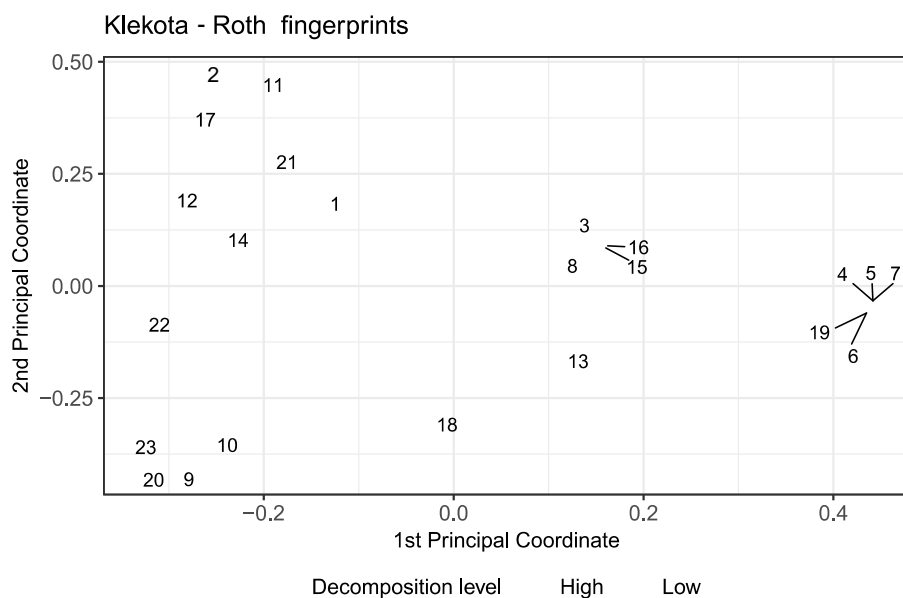
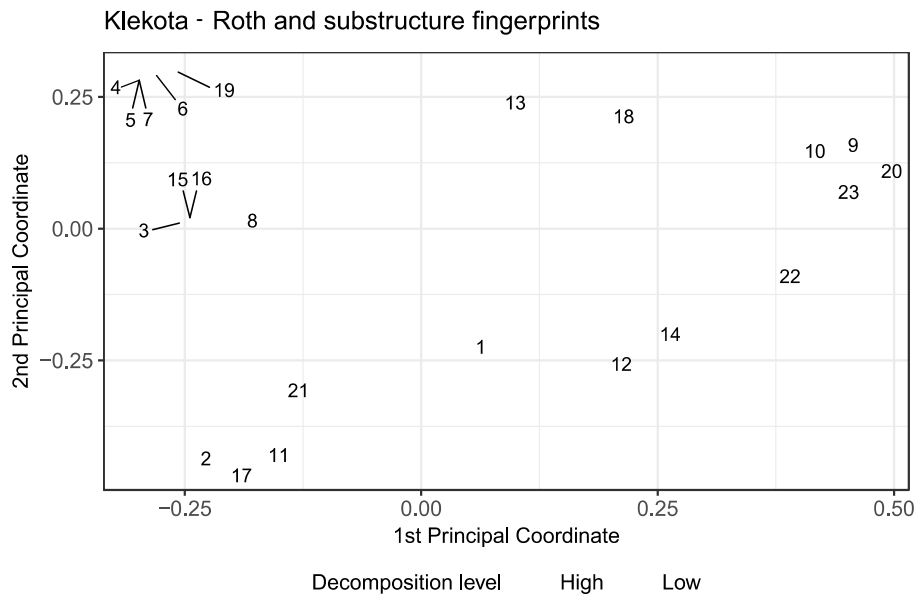Fig. 3. Score plot illustrating location of the compounds in the space of the Klekota–Roth fingerprint

Fig. 4. Score plot illustrating location of the compounds in the space of the substructure and Klekota–Roth fingerprint

Based on the calculated set of molecular fingerprints of the 23 samples a classification tree was derived with three decision nodes distributed over 3 levels (Fig. 10). Each node shows the predicted class (i.e. high or low decomposition level), the predicted

probability, and the percentage of observations in the node. The obtained decision tree is based on 3 descriptors and exhibits good agreement between observed and predicted data. The root node is defined by the presence/absence of rotatable bond in the cationic structure (SubFP302_c). The second node is defined by the presence/absence of aromatic N atom with 2 further total connections or aromatic N atom with a charge of +1, with 3 further total connections in cationic structure (SubFP181_c). The third node is defined by the presence/absence of primary carbon (SubFP1_c). Visualization of the chemical patterns can be found in the Supplementary Information.
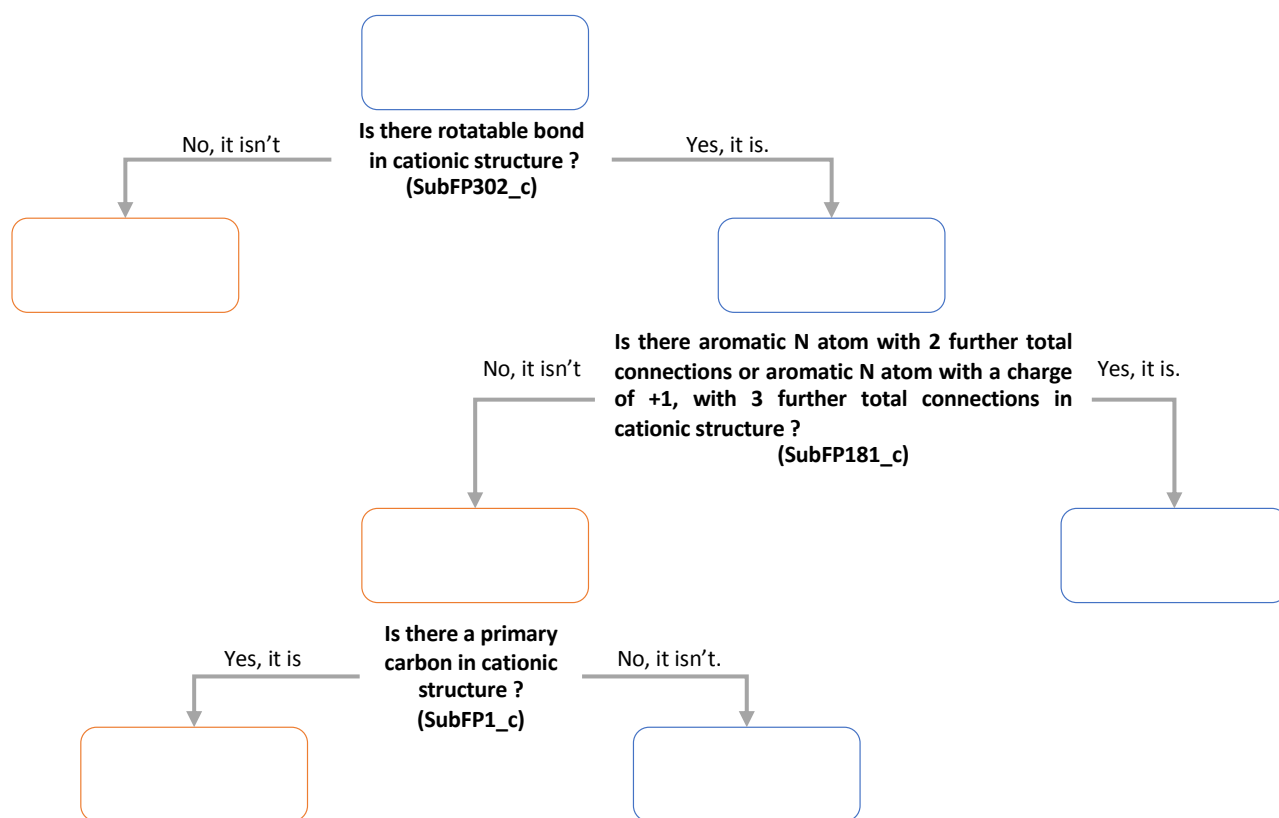

Fig. 5. Developed decision tree model

Almost all samples from the training set were correctly classified, which was showed in a confusion matrix (Fig. 11). Moreover, high values of metrics like accuracy (85%), sensitivity (100%), specificity (79%), precision (100%), and F-measure (1) confirmed goodof-fit of the model. Moreover, performed external validation (the developed model was used to predict the decomposition level for new samples) proved that the model has an acceptable predictive ability (Fig. 12). Only one new sample was classified incorrectly, which indicates that the presented decision tree could be a useful tool in the first stage of photocatalytic system design (Fig. 3). Prediction for all samples can be found in Table 2S in Supplementary Information.

		Predicted value	
		High level	Low level
Observed value	High level	6	0
	Low level	3	11

Figure 6 Confusion matrix describing the performance of a classification model on a training set

		Predicted value	
		High level	Low level
Observed value	High level	1	0
	Low level	1	1

Figure 7 Confusion matrix describing the performance of a classification model on a validation set

The developed decision tree model (Fig. 10) has indicated that the cation structure of IL's is the main contributor in IL-TiO$_2$ structure properties and plays a crucial role in its thermal stability under the conditions of synthesis. As earlier mentioned, the thermal stability under the condition of TiO$_2$ synthesis depends on (i) presence/absence of rotatable bond in the cationic structure (SubFP302_c), (ii) presence/absence of aromatic N atom with 2 further total connections or aromatic N atom with a charge of +1, with 3 further total connections in the cationic structure (SubFP181_c) and (iii) presence/absence of primary carbon (SubFP1_c). Schematic representation of each fingerprint can be found in the Supplementary Information.

(i)   Presence/absence of rotatable bond in the cationic structure (SubFP302_c)

The first descriptor in the developed decision tree, i.e. SubFP302_c (Fig. 10) has indicated that the presence of rotatable bonds in the cationic structure results in decreased decomposition level (i.e. higher thermal stability). It can be expected that the rotatability of bonds affords an enhanced degree of freedom to the molecule thereby lower steric hindrance that has implications on bonding formation between cation structure of IL and TiO$_2$ surface. Moreover, by rotation, neighbor atoms may decrease bonding distance

that will result in stronger bonds binding. In contrast, the absence of rotatable bond may result in higher steric collapse, lower binding energy and as a consequence in results lower energy needs for structure decomposition.

(ii)   Presence/absence of aromatic N atom with 2 further total connections or aromatic N atom with a charge of +1, with 3 further total connections in the cationic structure (SubFP181_c)

Thermal stability of ILs during solvothermal TiO_2 synthesis was found to be determined by the presence of heterocyclic containing N atom with 2 or 3 further connections (Fig. 13). This description concerns ionic liquid containing imidazolium, pyridinium, pyrrolidinium and tetrazolium cations. Indeed, experimental research, as well as quantum chemical, aided prediction of the thermal decomposition of pure ILs revealed that imidazolium derived ILs are generally the most stable salts followed by the other representatives: pyridinium, pyrrolidinium, piperidinium as well as tetraalkylammonium, phosphonium cations, etc. [50–52]. Moreover, pyrrolidinium-based derivatives were found to be more stable than pyridinium ones as observed based on the activation energy for thermal decomposition calculation [53]. Analogous observations were made in this study. According to Crosthwaite, ILs containing amino groups in the ring are more stable since these groups probably spread the charge more evenly around the ring [52]. Quantum chemical calculations performed by Kroon et al. revealed that ILs containing nucleophilic anions such as chloride undergo thermal decomposition by dealkylation of the cation (easiest accessible alkyl group) via SN2 reaction. For example, 1butyl-3-methylimidazolium cation is decomposed to 1butylimidazole rather than 1-methylimidazole, 1-butyl-1methylpyrrolidinium to 1-butylpyrrolidine, and pyridinium-based ILs into pyridine [53]. Formation of the 1-alkylimidazole rather than 1-methylimidazole may indicate that nucleophilic attack and subsequent thermolysis reactions primarily proceeded at the methyl group of IL [54]. Moreover, based on the imidazolium halides, Ohtani concluded that the attack of halide ions may also result in CAN bond cleavage providing alkenes, however previously described route is more preferential [54]. Decomposition of the imidazole ring was not observed up to 590°C confirming the stability of the imidazolium derivatives [55]. The analogous mechanism of SN2 dealkylation was also observed for tetraalkylammonium ILs which decompose towards trialkyl form of the compound [53].
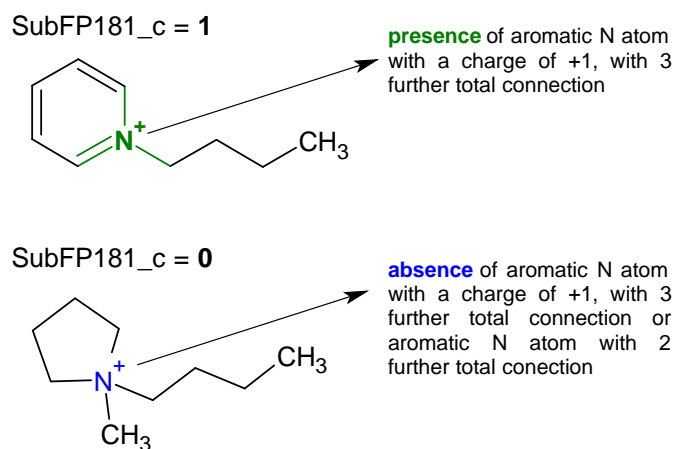

Figure   8   Example   illustrating   the   presence   and   absence   of   a   structural   fragment   called   SubFP181

(iii)   Presence/absence of primary carbon (SubFP1_c)

Selected descriptors that numerically represent IL's structure (Fig. 10) indicated that the presence of alkyl substituent in the morpholinium cation increases the thermal stability of the investigated compound since decomposing temperatures of morpholinium ILs are approximately 200°C, whereas morpholinium ring decomposes at 175–176°C [56,57]. Additional stability may also come from blocking the acidic hydrogen C2 in the second position of the imidazolium ring with alkyl group as shown for 1,3-didecyl2-methylimidazolium chloride [56]. Substitution in the C2position limits the possibility of the nucleophilic attack of the chloride anion and reactive carbenes formation, thus increasing the thermal stability. What is more, such substitution could also result in the steric hindrance and additional van der Waals forces. These factors may impede thermal degradation through the SN2 mechanism [58].

The length of the alkyl substituent in the IL's cation has a relatively small effect on thermal stability [58]. Generally, compounds with shorter chains were observed to have a slightly higher decomposition temperature [58]. The longer chain length increases the van der Waals interactions and decrease the charge density, thus limiting electrostatic interaction between cation and anion. Overall, it leads to lower thermal stability [58]. Moreover, the lower thermal stability of ILs with longer alkyl chain length may also be related to the increasing stability of linear, aliphatic carbocations and/or free radicals. In this regard, hydrocarbons with the increased chain length may be better leaving group in thermal decomposition of IL [59] (see Fig. 14).
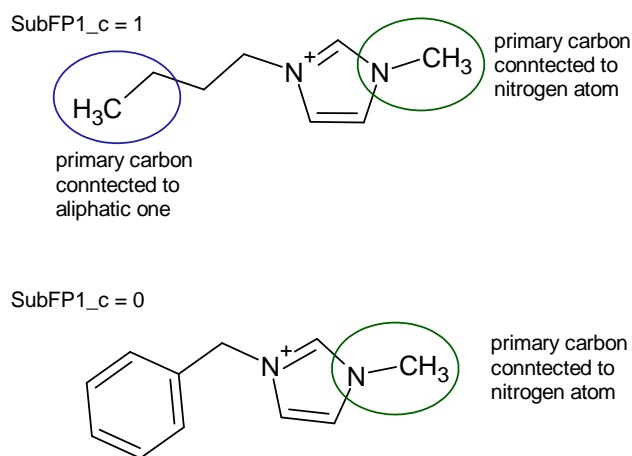

Figure 9 Example illustrating the presence of a structural fragment called "primary carbon"

In addition, based on both descriptors (i.e. presence/absence of rotatable bond in the cationic structure (SubFP302_c) and presence/absence of primary carbon, (SubFP1_c)) it can be expected that increased number of -CH3 group (SubFP302_c) and presence of rotatable bonds in the cationic structure (SubFP1_c) result in higher thermal stability in solvothermal reaction. The aliphatic R-groups afford higher rotatability of bonds than R-groups in aromatic rings that increases thermal stability of IL-TiO$_2$ structures in solvothermal reaction.

5. Conclusions

Contrary, to studies reporting excitation mechanism of TiO$_2$ obtained in the presence of ionic liquids [60–63], in this study we have tried to gain a deeper insight into the photocatalytic activity of ILs-TiO$_2$ photocatalysts by incorporating computational methods. Thus, in the present study, we have applied for the first time the chemoinformatic analysis combined with experimental results to find the relationship between the structure of the ionic liquid, its thermal stability under the conditions of TiO$_2$ synthesis and photocatalytic activity of ILs-TiO$_2$ photocatalysts. The developed model provides information about the structural features of ionic liquids responsible for thermal stability during synthesis. These are the presence/absence of heterocyclic containing N atom with 2 or 3 further connections, primary carbon, and rotatable bond in the cationic structure. The presence/absence of these structural features could be treated as the primary selection criteria for potential ionic liquids in the process of the design and synthesis of an efficient IL-TiO$_2$-based photocatalyst. Moreover, based on the predicted value, we can assume which mechanism of photoexcitation under Vis for the new samples modified with ionic liquids will occur. This information is essential for further work on the synthesis of IL-TiO$_2$ photocatalyst. Finally, the described stage of experimental procedure supported by theoretical methods is the first step in the development of a comprehensive methodology for the design of a safer and more efficient IL-TiO$_2$ based photocatalyst. The developed model allows predicting the property of ionic liquids (thermal stability) that influences the efficiency of the IL-TiO$_2$ system. We do believe that the presented approach provides information about essential structural features that may lead to increased efficiency of newly designed IL-TiO$_2$-based photocatalytic materials. The integration of designed synthesis [25–30] and findings derived from computational study could reduce the number and cost of necessary experiments and make the experimental process more effective. Moreover, further work on the development of the methodology of photocatalyst design supported by the computational study should be extended i.e. in terms of selection of the optimal ionic liquids characterized by specific structural features, physicochemical properties, and low toxicity towards various organisms.

6. Author contributions

T.P, A.M, A.R-F. was responsible for conceptualization of the project. A.R-F., A.M. designed the research, analyzed the experimental data, performed the computational part of study, prepared discussion of the results and the final version of the manuscript; A. M, A.R-F., J. Ł took part in writing the final version of the manuscript; J.Ł, A. Z-M, M. P-G, M.P performed the experimental work. All authors took part in editing and have given approval to the final version of the manuscript.

7. Conflict of interest

The authors declare that they have no known competing financial interests or personal relationships that could have appeared to influence the work reported in this paper.

8. Acknowledgments

9. References

[1] A. Fujishima, N.R. Tata, D.A. Tryk, Titanium dioxide photocatalysis, J. Photochem. Photobiol. C Photochem. Rev. 1 (2000) 1–21, https://doi.org/10.1016/S1389-5567(00)00002-2.

[2] B. Ohtani, Photocatalysis A to Z—What we know and what we do not know in a scientific sense, J. Photochem. Photobiol. C Photochem. Rev. 11 (2010) 157–178, https://doi.org/10.1016/j.jphotochemrev.2011.02.001.

[3] K. Nakata, A. Fujishima, TiO2 photocatalysis: Design and applications, J. Photochem. Photobiol. C Photochem. Rev. 13 (2012) 169–189, https://doi.org/10.1016/j.jphotochemrev.2012.06.001.

[4] M.A. Fox, M.T. Dulay, Heterogeneous photocatalysis, Chem. Rev. 93 (1993) 341–357, https://doi.org/10.1021/cr00017a016.

[5] J. Schneider, M. Matsuoka, M. Takeuchi, J. Zhang, Y. Horiuchi, M. Anpo, D.W. Bahnemann, Understanding TiO2 photocatalysis: mechanisms and materials, Chem. Rev. 114 (2014) 9919–9986, https://doi.org/10.1021/cr5001892.

[6] Q. Wang, K. Domen, Particulate photocatalysts for light-driven water splitting: mechanisms, challenges, and design strategies, Chem. Rev. 120 (2020) 919–985, https://doi.org/10.1021/acs.chemrev.9b00201.

[7] D. Fattakhova-Rohlfing, A. Zaleska, T. Bein, Three-dimensional titanium dioxide nanomaterials, Chem. Rev. 114 (2014) 9487–9558, https://doi.org/10.1021/cr500201c.

[8] Y. Shu, X. Gong, Z. Jiang, L. Lu, X. Xu, C. Wang, H. Deng, Metal-organic frameworks for the exploit of distance between active sites in efficient photocatalysis, Angew. Chemie Int. Ed. (2020), https://doi.org/10.1002/ anie.201915537.

[9] K. Shirai, G. Fazio, T. Sugimoto, D. Selli, L. Ferraro, K. Watanabe, M. Haruta, B. Ohtani, H. Kurata, C. Di Valentin, Y. Matsumoto, Water-assisted hole trapping at the highly curved surface of nano-TiO2 photocatalyst, J. Am. Chem. Soc. 140 (2018) 1415–1422, https://doi.org/10.1021/jacs.7b11061.

[10] M.F. Kuehnel, C.E. Creissen, C.D. Sahm, D. Wielend, A. Schlosser, K.L. Orchard, E. Reisner, ZnSe nanorods as visible-light absorbers for photocatalytic and photoelectrochemical H2 evolution in water, Angew. Chemie Int. Ed. 58 (2019) 5059–5063, https://doi.org/10.1002/anie.201814265.

[11] S. Banerjee, S.C. Pillai, P. Falaras, K.E. O'Shea, J.A. Byrne, D.D. Dionysiou, New insights into the mechanism of visible light photocatalysis, J. Phys. Chem. Lett. 5 (2014) 2543–2554, https://doi.org/10.1021/jz501030x.

[12] S.G. Kumar, L.G. Devi, Review on modified TiO2 photocatalysis under UV/ visible light: selected results and related mechanisms on interfacial charge carrier transfer dynamics, J. Phys. Chem. A 115 (2011) 13211–13241, https:// doi.org/10.1021/jp204364a.

[13] X. Yang, D. Wang, Photocatalysis: from fundamental principles to materials and applications, ACS Appl. Energy Mater. 1 (2018) 6657–6693, https://doi.org/10.1021/acsaem.8b01345.

[14] R. Asahi, T. Morikawa, H. Irie, T. Ohwaki, Nitrogen-doped titanium dioxide as visible-light-sensitive photocatalyst: designs, developments, and prospects, Chem. Rev. 114 (2014) 9824–9852, https://doi.org/10.1021/cr5000738.

[15] X. Chen, S.S. Mao, Titanium dioxide nanomaterials: synthesis, properties, modifications, and applications, Chem. Rev. 107 (2007) 2891–2959, https://doi.org/10.1021/cr0500535.

[16] R. Daghrir, P. Drogui, D. Robert, Modified TiO2 for environmental photocatalytic applications: a review, Ind. Eng. Chem. Res. 52 (2013) 3581–3599, https://doi.org/10.1021/ie303468t.

[17] A. Mikolajczyk, A. Gajewicz, E. Mulkiewicz, B. Rasulev, M. Marchelek, M. Diak, S. Hirano, A. Zaleska-Medynska, T. Puzyn, Nano-QSAR modeling for ecosafe design of heterogeneous TiO2 -based nano-photocatalysts, Environ. Sci. Nano. 5 (2018) 1150–1160, https://doi.org/10.1039/C8EN00085A.

[18] A. Mikolajczyk, A. Malankowska, G. Nowaczyk, A. Gajewicz, S. Hirano, S. Jurga, A. Zaleska-Medynska, T. Puzyn, Combined experimental and computational approach to developing efficient photocatalysts based on Au/Pd–TiO2 nanoparticles, Environ. Sci. Nano 3 (2016) 1425–1435, https://doi.org/10.1039/C6EN00232C.

[19] A. Krukowska, M.J. Winiarski, J. Strychalska-Nowak, T. Klimczuk, W. Lisowski, A. Mikolajczyk, H.P. Pinto, T. Puzyn, T. Grzyb, A. Zaleska-Medynska, Rare earth ions doped K2Ta2O6 photocatalysts with enhanced UV–vis light activity, Appl. Catal. B Environ. 224 (2018) 451–468, https://doi.org/10.1016/j.apcatb.2017.10.061.

[20] A. Cybula, J.B. Priebe, M.-M. Pohl, J.W. Sobczak, M. Schneider, A. Zielin´ skaJurek, A. Brückner, A. Zaleska, The effect of calcination temperature on structure and photocatalytic properties of Au/Pd nanoparticles supported on TiO2, Appl. Catal. B Environ. 152–153 (2014) 202–211, https://doi.org/ 10.1016/j.apcatb.2014.01.042.

[21] J. Luczak, M. Paszkiewicz, A. Krukowska, A. Malankowska, A. ZaleskaMedynska, Ionic liquids for nano- and microstructures preparation. Part 1: Properties and multifunctional role, Adv Colloid Interface Sci. 230 (2016) 13–28, https://doi.org/10.1016/j.cis.2015.08.006.

[22] J. Luczak, M. Paszkiewicz, A. Krukowska, A. Malankowska, A. ZaleskaMedynska, Ionic liquids for nano- and microstructures preparation. Part 2: Application in synthesis, Adv Colloid Interface Sci. 227 (2016) 1–52, https:// doi.org/10.1016/j.cis.2015.08.010.

[23] P.A. Hunt, B. Kirchner, T. Welton, Characterising the electronic structure of ionic liquids: an examination of the 1-butyl-3-methylimidazolium chloride ion pair, Chemistry (Easton) 12 (2006) 6762–6775, https://doi.org/10.1002/ chem.200600103.

[24] H. Weingartner, Understanding ionic liquids at the molecular level: facts, problems, and controversies, Angew. Chem. Int. Ed. Engl. 47 (2008) 654–670, https://doi.org/10.1002/anie.200604951.

[25] J. Łuczak, M. Paszkiewicz-Gawron, M. Długokęcka, W. Lisowski, E. Grabowska, S. Makurat, J. Rak, A. Zaleska-Medynska, Visible-light photocatalytic activity of ionic liquid TiO2 spheres: effect of the ionic liquid's anion structure, ChemCatChem 9 (2017) 4377–4388, https://doi.org/10.1002/cctc.201700861.

[26] M. Paszkiewicz-Gawron, M. Długokęcka, W. Lisowski, M.C. Paganini, E. Giamello, T. Klimczuk, M. Paszkiewicz, E. Grabowska, A. Zaleska-Medynska, J. Luczak, Dependence between ionic liquid structure and mechanism of visible-light-induced activity of TiO2 obtained by ionic-liquid-assisted solvothermal synthesis, ACS Sustain. Chem. Eng. 6 (2018) 3927–3937, https://doi.org/10.1021/acssuschemeng.7b04291.

[27] M. Paszkiewicz, J. Łuczak, W. Lisowski, P. Patyk, A. Zaleska-Medynska, The ILsassisted solvothermal synthesis of TiO2 spheres: The effect of ionic liquids on morphology and photoactivity of TiO2, Appl. Catal. B Environ. 184 (2016) 223– 237, https://doi.org/10.1016/j.apcatb.2015.11.019.

[28] M. Paszkiewicz-Gawron, A. Gołąbiewska, A. Pancielejko, W. Lisowski, J. Zwara, M. Paszkiewicz, A. Zaleska-Medynska, J. Łuczak, Impact of tetrazolium ionic liquid thermal decomposition in solvothermal reaction on the remarkable photocatalytic properties of TiO2 particles, Nanomaterials 9 (2019) 744, https://doi.org/10.3390/nano9050744.

[29] A. Gołąbiewska, M. Paszkiewicz-Gawron, A. Sadzin´ ska, W. Lisowski, E. Grabowska, A. Zaleska-Medynska, J. Łuczak, Fabrication and photoactivity of ionic liquid–TiO2 structures for efficient visible-light-induced photocatalytic decomposition of organic pollutants in aqueous phase, Beilstein J. Nanotechnol. 9 (2018) 580–590, https://doi.org/10.3762/bjnano.9.54.

[30] A. Gołąbiewska, M. Checa-Suárez, M. Paszkiewicz-Gawron, W. Lisowski, E. Raczuk, T. Klimczuk, Z. Polkowska, E. Grabowska, A. Zaleska-Medynska, J._ Łuczak, Highly active TiO2 microspheres formation in the presence of ethylammonium nitrate ionic liquid, Catalysts 8 (2018) 279, https://doi.org/ 10.3390/catal8070279.

[31] C. Creutz, B.S. Brunschwig, N. Sutin, Interfacial charge-transfer absorption: semiclassical treatment, J. Phys. Chem. B 109 (2005) 10251–10260, https://doi.org/10.1021/jp050259+.

[32] C. Creutz, B.S. Brunschwig, N. Sutin, Interfacial charge transfer absorption: Application to metal–molecule assemblies, Chem. Phys. 324 (2006) 244–258, https://doi.org/10.1016/j.chemphys.2005.12.015.

[33] C. Creutz, B.S. Brunschwig, N. Sutin, Interfacial charge-transfer absorption: 3. Application to semiconductor molecule assemblies, J. Phys. Chem. B. 110 (2006) 25181–25190, https://doi.org/10.1021/jp063953d.

[34] A. Mauri, V. Consonni, M. Pavan, R. Todeschini, DRAGON software: an easy approach to molecular descriptor, Commun. Math. Comput. Chem. (2006) 237– 248 (accessed March 13, 2019).

[35] C.W. Yap, PaDEL-descriptor: An open source software to calculate molecular descriptors and fingerprints, J. Comput. Chem. 32 (2011) 1466–1474, https:// doi.org/10.1002/jcc.21707.

[36] J. Miller, J.C. Miller, Statistics and Chemometrics for Analytical Chemistry, 7th ed., Pearson Education Limited, 2018.

[37] J.H. Ward, Hierarchical grouping to optimize an objective function, J. Am. Stat. Assoc. 58 (1963) 236–244, https://doi.org/10.1080/ 01621459.1963.10500845.

[38] K. Odziomek, A. Rybinska, T. Puzyn, Unsupervised learning methods and similarity analysis in chemoinformatics, in: J. Leszczynski (Ed.), Handb. Comput. Chem., Springer International Publishing, Cham, 2017, pp. 2095– 2132, https://doi.org/10.1007/978-3-319-27282-5_53.

[39] A.C.D. Inc., Advanced Chemistry Development Inc., ACD/ChemSketch, 2010. www.acdlabs.com (accessed April 17, 2014).

[40] J. Gasteiger (Ed.), Handbook of Chemoinformatics, Wiley-VCH Verlag GmbH, Weinheim, Germany, 2003, https://doi.org/10.1002/ 9783527618279.

[41] A. Steffen, T. Kogej, C. Tyrchan, O. Engkvist, Comparison of molecular fingerprint methods on the basis of biological profile data, J. Chem. Inf. Model. 49 (2009) 338–347, https://doi.org/10.1021/ci800326z.

[42] K. Rataj, W. Czarnecki, S. Podlewska, A. Pocha, A. Bojarski, Substructural connectivity fingerprint and extreme entropy machines—a new method of compound representation and analysis, Molecules 23 (2018) 1242, https://doi. org/10.3390/molecules23061242.

[43] R. Wehrens, Chemometrics with R, Springer Berlin Heidelberg, Berlin, Heidelberg, 2011. 10.1007/978-3-642-17841-2.

[44] R.G. Brereton, Chemometrics for Pattern Recognition, John Wiley & Sons Ltd, Chichester, UK, 2009. 10.1002/9780470746462.

[45] Y. Xu, F. Gong, S.J. Dixon, R.G. Brereton, H.A. Soini, M.V. Novotny, E. Oberzaucher, K. Grammer, D.J. Penn, Application of dissimilarity indices, principal coordinates analysis, and rank tests to peak tables in metabolomics of the gas chromatography/mass spectrometry of human sweat, Anal. Chem. 79 (2007) 5633–5641, https://doi.org/10.1021/ac070134w.

[46] R Development Core Team, R: A Language and Environment for Statistical Computing 1 (2016) 409. 10.1007/978-3-540-74686-7.

[47] K. Roy, S. Kar, R.N. Das, Understanding the Basics of QSAR for Applications in Pharmaceutical Sciences and Risk Assessment, Elsevier Academic Press, Amsterdam, Boston, 2015.

[48] A. Gajewicz, T. Puzyn, K. Odziomek, P. Urbaszek, A. Haase, C. Riebeling, A. Luch, M.A. Irfan, R. Landsiedel, M. van der Zande, H. Bouwmeester, Decision tree models to classify nanomaterials according to the DF4 nano grouping scheme, Nanotoxicology 12 (2018) 1–17, https://doi.org/10.1080/17435390. 2017.1415388.

[49] OECD, OECD principles for the validation, for regulatory purposes, of Quantitative Structure-Activity Relationship models, in: Paris, 2004. http:// www.oecd.org/chemicalsafety/risk-assessment/37849783.pdf (accessed April 18, 2014).

[50] E. Maria Siedlecka, M. Czerwicka, S. Stolte, P. Stepnowski, Stability of ionic liquids in application conditions, Curr. Org. Chem. 15 (2011) 1974–1991, https://doi.org/10.2174/138527211795703630.

[51] H. Tokuda, K. Ishii, A. Bin, H. Susan, S. Tsuzuki, K. Hayamizu, M. Watanabe, M.A. B.H. Susan, S. Tsuzuki, K. Hayamizu, M. Watanabe, Physicochemical properties and structures of room-temperature ionic liquids. 3. Variation of cationic structures, J. Phys. Chem. B 110 (2006) 2833–2839, https://doi.org/10.1021/ jp053396f.

[52] J.M. Crosthwaite, M.J. Muldoon, J.K. Dixon, J.L. Anderson, J.F. Brennecke, Phase transition and decomposition temperatures, heat capacities and viscosities of pyridinium ionic liquids, J. Chem. Thermodyn. 37 (2005) 559–568, https://doi. org/10.1016/j.jct.2005.03.013.

[53] M.C. Kroon, W. Buijs, C.J. Peters, G.-J. Witkamp, Quantum chemical aided prediction of the thermal decomposition mechanisms and temperatures of ionic liquids, Thermochim. Acta 465 (2007) 40–47, https://doi.org/10.1016/j. tca.2007.09.003.

54] H. Ohtani, S. Ishimura, M. Kumai, Thermal decomposition behaviors of imidazolium-type ionic liquids studied by pyrolysis-gas chromatography, Anal. Sci. 24 (2008) 1335–1340. http://www.ncbi.nlm.nih.gov/pubmed/ 18845896.

55] Chemical Book Inc., n.d. https://www.chemicalbook.com/ChemicalProductProperty_EN_CB6460617.htm (accessed February 11, 2019).

56] J.G. Huddleston, A.E. Visser, W.M. Reichert, H.D. Willauer, G.A. Broker, R.D. Rogers, Characterization and comparison of hydrophilic and hydrophobic room temperature ionic liquids incorporating the imidazolium cation, Green Chem. 3 (2001) 156–164, https://doi.org/10.1039/b103275p.

57] M. Williams, The Merck index: an encyclopedia of chemicals, drugs, and biologicals, Drug Dev. Res. 67 (2006), https://doi.org/10.1002/ddr.20159. 870– 870.

58] Y. Cao, T. Mu, Comprehensive investigation on the thermal stability of 66 ionic liquids by thermogravimetric analysis, Ind. Eng. Chem. Res. 53 (2014) 8651– 8664, https://doi.org/10.1021/ie5009597.

59] M. Montanino, M. Carewska, F. Alessandrini, S. Passerini, G.B. Appetecchi, The role of the cation aliphatic side chain length in piperidinium bis (trifluoromethansulfonyl)imide ionic liquids, Electrochim. Acta 57 (2011) 153–159, https://doi.org/10.1016/j.electacta.2011.03.089.

[60] J. Huang, C. Qin, S. Lei, J. Li, M. Li, J. Zhong, T. Wang, Ionic liquid assisted hydrothermal preparation of TiO2 with largely enhanced photocatalytic performance originated from effective separation of photoinduced carriers, J. Phys. Chem. Solids 139 (2020) 109323, https://doi.org/10.1016/j.jpcs.2019.109323.

[61] T.N. Ravishankar, M. do O. Vaz, T. Ramakrishnappa, S.R. Teixeira, J. Dupont, Ionic liquid–assisted hydrothermal synthesis of Nb/TiO2 nanocomposites for efficient photocatalytic hydrogen production and photodecolorization of Rhodamine B under UV-visible and visible light illuminations, Mater. Today Chem. 12 (2019) 373–385, https://doi.org/10.1016/j.mtchem.2019.04.001.

[62] K. Manjunath, L.S. Reddy Yadav, T. Jayalakshmi, V. Reddy, H. Rajanaika, G. Nagaraju, Ionic liquid assisted hydrothermal synthesis of TiO2 nanoparticles: photocatalytic and antibacterial activity, J. Mater. Res. Technol. 7 (2018) 7–13, https://doi.org/10.1016/j.jmrt.2017.02.001.

[63] L. Qi, J. Yu, M. Jaroniec, Enhanced and suppressed effects of ionic liquid on the photocatalytic activity of TiO2, Adsorption 19 (2013) 557–561, https://doi.org/10.1007/s10450-013-9478-7.